BUFFET AND BUFFETING CHARACTERISTICS OF HIGH AGILITY AND TRANSPORT AIRCRAFT

C. Breitsamter

Technical University of Munich, Chair of Aerodynamics and Fluid Mechanics, Boltzmannstr. 15, 85748 Garching

Abstract

Unsteady aerodynamic excitation of aircraft wing and tail surfaces may evoke from separated and turbulent flows induced by shock boundary layer interactions, burst leading-edge vortex flow structures or airbrake turbulent wake flow. The corresponding excitation of the wing and/or tail structures due to unsteady aerodynamic forces is referred to as 'buffet'. While for transonic transport aircraft shock induced flow separation at off-design conditions constitutes buffet, the separated flow associated with burst leading-edge and strake vortices is the dominant mechanism for buffet at high agility aircraft. The dominating turbulent flow fields associated with shock induced flow separation or burst large-scale vortices can cause severe surface pressure fluctuations both on the wing itself and on downstream components, particularly, the horizontal and/or vertical stabilizers. The structural response of the aircraft is denoted as 'buffeting'. Buffeting can have serious impacts on the aircraft, resulting in increased structural vibrations and high accelerations in the area of wing and tail tip sections, structural maximum and fatigue loads, and degraded flight characteristics. Buffeting, with its interaction of unsteady aerodynamic forces, inertia forces, and elastic forces, represents a dynamic aeroelastic response problem. It is treated as limitation of the flight envelope in verification and certification processes. Unsteady aerodynamic forces consists of flow separation dependent aerodynamic forces (shock induced or due to vortex bursting) and motion induced aerodynamic forces (oscillations of the elastic structures in their eigenmodes). Due to its significance as a flight envelope limit and the complex coupling mechanisms between flow scenarios and structural properties, buffeting has been a subject of research in the field of aeroelasticity from the very beginning. This overview paper addresses some main mechanisms of vortex-induced and shock-induced buffet flow. Associated fluctuation intensities of surface pressures are reported and surface pressure frequency characteristics related to fluid mode instabilities are analyzed. Semi-empirical relations to quantify buffet onset and buffet intensity levels are further given.

1. INTRODCUTION

Flight envelope limits are associated with dynamic aeroelastic phenomena. Determining such limits as accurately as possible is a key task in the design and certification process of aircraft. Those limiting phenomena are characterized by the coupling of unsteady aerodynamic, structural-elastic, and inertia forces as displayed in Fig.1. Dynamic aeroelasticity problems can be structured in stability and response problems. The stability problem manifests itself in self-excited, and in the crucial case, undamped oscillations of structural eigenmodes, which is referred to as flutter and can lead to explosive-like fracture of wing or tail structures. If the amplitudes of the structural deformations remain limited, they are referred to as limit cycle oscillations. In contrast, response problems are typically linked to phenomena denoted as buffeting, buzz and gust impact. Buffeting is described by pilots as 'shaking phenomena', where pronounced oscillations of wing and/or tail surfaces are evoked by locally separated flow due to bursting of leading-edge vortices or by shocks with the latter undergoing motions accompanied by separated flow. Buzz appears also with shock motions and induced flow separation resulting in control surface oscillations with limited amplitude. The impact of gusts represents a classical dynamic response problem. Gust evolution is linked to atmospheric and weather conditions.

Focusing on buffeting, Fig. 2 shows a block diagram of the structural dynamics system (mass, damping and stiffness features) performing structural motions or oscillations, respectively, linked to motion induced aerodynamic forces. Flow separation induced aerodynamic forces are acting on the system as additional excitation quantities. Interaction characteristics between motion- and separation-induced aerodynamic forces depends on the specific

problem. Consequently, the term 'Buffet' refers to the aerodynamic excitation while 'Buffeting' denotes the coupled problem including the structural response.

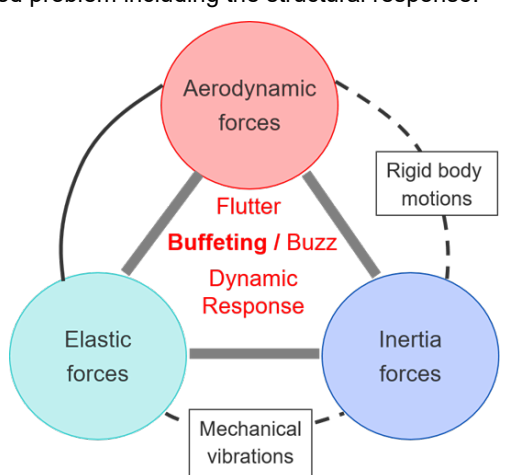


FIG 1. Aeroelastic force triangle (Collar's triangle), cf. [1].

1.1. Buffeting on High Agility Aircraft

Addressing high-agility aircraft associated with the development of leading-edge vortices, buffeting may generally occur on wing and horizontal and vertical tail surfaces, respectively. The corresponding unsteady aerodynamic loads, i.e. Buffet, are caused by the separated and unsteady flow linked to the bursting mechanism of leading-edge vortices [2]. Especially, the fin buffeting problem is a critical issue for high performance fighter aircraft equipped with twin vertical tails [3], single fin configurations could be affected as well [4].

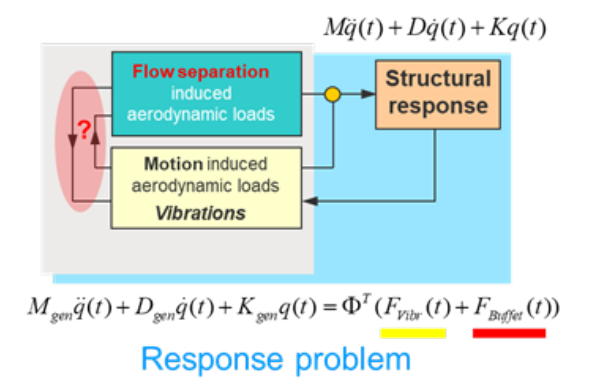


FIG 2. Buffeting Block diagram (t: time, q(t): surface displacement variable; M, D, K: mass, damping stiffness (matrices); F: aerodynamic forces; index *gen*: generalized terms with respect to a modal description applying generalized aerodynamic force matrices; Φ: modal matrix [12]).

The highly turbulent flow caused by the bursting of leading-edge vortices occur mainly at high angles of attack. Strong large-scale vortices are shed at slender wing geometries, such as delta wing planforms, strakes or leading-edge extensions [5]. Leading-edge vortices in a fully developed, stable stage improve significantly maneuver capabilities because of additional lift and an increase in maximum angle of attack. However, leading-edge vortices are subject to breakdown at high angles of attack [5], [6]. The breakdown flow leads to high turbulence levels in line with specific instability mechanisms resulting in narrow-band unsteady aerodynamic forces [2], [7]. Such loads often excite the vertical tail structure in its natural frequencies causing increased fatigue loads and reduced service life and raise maintenance costs [8]. Comprehensive studies had been carried out on the fin buffeting problem including also methods for flow control and active vibration alleviation [9], [10], [11].

1.2. Buffeting on Transonic Transport Aircraft

Regarding so-called 'off-design' conditions for transport aircraft featuring supercritical wings, prevailing shock fluctuations on the wing in the chord and span directions, combined with shock-induced, locally separated flow, can lead to buffeting [13], [14]. Transonic buffeting is characterized by a pronounced shock-boundary layer interaction, resulting in shock-induced downstream and outboard regions of flow separation [15]. This is linked to a selfsustaining shock motion, which interacts with the dynamically developing region of separated flow. It results in flow conditions of varying complexity on airfoils and swept wings with finite aspect ratios [14]. Based on the results of various numerical and experimental studies, buffeting on the wing is caused by the interaction of various physical mechanisms. Stability analyses based on linearized Unsteady Reynolds-averaged Navier-Stokes equations (URANS) show the presence of global flow instabilities [16], [17], [18]. On the one hand, there is a mode associated with the shock motion in the chord direction (Strouhal number based on wing mean chord: Sr $\approx 0.05 - 0.1$), and on the other hand, modes associated with the propagation of so-called 'buffet cells' in the spanwise direction (Sr \approx 0.2 – 0.6; propagation velocity: $u/u_{ref} \approx$ 0.25 - 0.5) [15], [17]. The characteristic frequencies are more broadband on the finite aspect ratio wing compared to those on airfoils [19]. Representing numerically shock motion and shock-induced flow separation, at least URANS methods often combined with zonal scale-resolving approaches such as (D)DES ('(Delayed) Detached Eddy Simulations') are typically used [20].

Numerical and experimental studies with predefined rigid-body motions or structural vibrations set at airfoils test cases show that, at sufficiently large vibration amplitudes, a 'lock-in effect' of the buffet and vibration frequencies occurs [21]. This is also evident in corresponding scenarios of elastically supported airfoils [22], [23]. Overall, structural vibrations can therefore affect the buffet-specific aerodynamic excitation due to an interaction of motionand separation-induced unsteady aerodynamic forces [27] (see also Fig. 2). Further, coupled fluid-structural simulations (comparison of one- and two-way coupling methods [12]) are performed to elucidate the interaction mechanisms in detail.

As additional aspects, the application of URANS/(D)DES methods to simulate buffet flows is not feasible for the multitude of parameters that must be varied in an aircraft design process due to the computational requirements. Even with current high-performance computing power, they can only be applied to selected cases. Furthermore, calculating buffeting requires a coupling between the flow solver and the structural solver, which generates additional computational effort. Therefore, especially with regard to industrial applications, a compromise must be reached between the desired physical accuracy and the resulting computational costs. One way to reduce the computational effort is the use of reduced-order models (ROMs), which are trained and validated using CFD simulation data or experimental data sets. The trained model can then be applied to other inflow conditions to predict characteristic aerodynamic and aeroelastic quantities, respectively. Consequently, the computational effort of aeroelastic investigations can be significantly reduced. Recent developments have been conducted to capture buffet related spatially and temporally varying surface pressure distributions on a typical transport aircraft applying specific ROMs [24]. The ROMs employ convolutional neural networks and use auto-encoders to address spatial variations and are linked to long short-term memory neural networks for transient predictions [25-27].

2. VORTEX BURSTING BUFFET

Buffet and buffeting characteristics affecting high agility aircraft are highlighted in the following presenting an overview on some dominant mechanisms. These findings have been partially published by the author in Ref. [2].

2.1. Unsteady flow field - Buffet impact

Flow properties of leading-edge vortices developing at highly swept wing geometries related especially to single or multi-swept delta wings and strake elements are discussed in a wide body of literature [5]. Vortex evolution stages, influence of wing planform and airfoil parameters (sharp or round leading-edges, thickness, camber) along with Mach number and Reynolds number dependencies are reported in detail. Further, characteristics of vortex-vortex and vortex-shock interactions present at hybrid delta wings featuring multi-swept leading-edges are studied. For all those cases, vortex bursting takes place at high angles of attack constituting the highly unsteady and

turbulent flowfield acting on wing and tail surfaces, thus, representing the buffet conditions.

Wing leading-edge vortex breakdown is of the spiral type for Reynolds numbers of Re > 104 and typical swirl numbers present at delta wing vortices. Fig. 3 highlights the vortex flow characteristics taken at a delta wing of 76° leading-edge sweep (aspect ratio 1) for low speed flow conditions and angle of attack of $\alpha = 35^{\circ}$. Vortex bursting takes place approximately at $x/c_r = 0.49$ (c_r: wing root chord). Next to the original jet-like vortex core a region of strong flow deceleration occurs that vortex breakdown is caused by the stagnation of the axial core flow. The region of retarded axial core flow is caused by the adverse pressure gradient arising at high angle of attack [2], [5]. The corresponding steep velocity gradients and the rapid change from jet-like to wake-like core flow evokes an overall maximum in turbulence intensity at the vortex center. The peak turbulence intensities are indicated in Fig. 3 by root mean square values (rms) of axial velocity fluctuations normalized with the freestream velocity U... Peak rms levels are up to 35%. Downstream of the burst location, the region of maximum turbulence intensity expands rapidly in radial direction. The associated local turbulence maxima are located in a limited radial range around the burst vortex core. This area corresponds to the points of inflection in the radial profiles of the retarded axial core flow.

Analyzing the spectral content of the velocity fluctuations it is shown that the breakdown flow exhibits a significant spectral peak indicating that turbulent kinetic energy is channeled into a narrow band. The frequency related to this spectral peak is named 'dominant frequency'. The energy concentration in a limited frequency range is linked to a specific instability mechanism called helical mode instability of the breakdown flow [2], [7]. Consequently, quasi–periodic aerodynamic loads occur which are prone to excite structural modes.

2.2. Fin surface pressures

The impingement of burst leading-edge vortices is a source of buffet excitation on an aircraft experienced on the wing surface or on other surfaces such as the fin.

2.2.1. Fluctuation intensities

The vortex breakdown highly turbulent flowfield gives rise to surface pressure fluctuations for the areas affected by the impingement. Thus, the buffet excitation can be quantified by the corresponding pressure fluctuation intensities (rms values) present on the respective surfaces. Exemplarily, the vertical tail (single fin) of a delta-canard high agility aircraft is considered as shown in Fig. 4. Measurements have been conducted on a 1:15 scaled wind tunnel model at low-speed flow conditions for an angle of attack sweep from $\alpha = 0^{\circ}$ to 31.2° [2], [10]. Based on 18 differential unsteady pressure transducers (Kulites) the surface-averaged rms values of the pressure fluctuations are determined and plotted as pressure coefficient data, c_{p,rms}, for the angle-of-attack sweep. The rms values increase significantly above $\alpha = 20^{\circ}$ reaching a value of about 8% at maximum angle of attack of $\alpha \approx 30^{\circ}$. The severe increase in the rms pressures above a certain incidence is a characteristic feature of the fin buffet phenomenon. It is observed at most high agility aircraft and, in particular, becomes critical on twin-fin configurations where the fins are often fully impinged by the vortex breakdown flow.

2.2.2. Frequency characteristics

The amplitude spectra of the fluctuating surface pressures, calculated from the signal taken at sensor station P13, are shown in Fig. 5 for all angles of attack considered. Above $\alpha \approx 22^{\circ}$, spectral peaks can be identified in the range of reduced frequencies of k = 0.8 -0.6 (k = $f \cdot l_{\mu}/U_{\infty}$; f: frequency, Hz; l_{μ} : wing mean aerodynamic chord, m; U∞: freestream velocity, m/s). The helical mode instability of the burst wing leading-edge vortices starts to affect the fin pressure field and the narrow-band amplitude increases strongly from $\alpha = 24^{\circ}$ to $\alpha = 31.2^{\circ}$. This energy peak is called 'buffet peak'. Hence, the narrow-band concentration of turbulent kinetic energy may result in strong excitation of structural modes. It can be further detected that the reduced frequencies associated with the buffet peak, i.e. the dominant frequencies, are shifted to lower values at higher angles of attack. This trend is found for various configurations, cf. [28], [29].

2.3. Fin buffeting phenomena

Such pressure distributions create the buffeting, or structural response to the buffet. The resulting fin buffeting mainly consists of a response in the first bending and torsion mode. As an example, Fig. 6 (left) shows the impact of the strong vortices shed at the leading-edge extensions (LEX: strake elements) of the F-18 high angleof-attack research aircraft. Thus, the fluid-structure interactions of vortex breakdown with a fin involves the following phenomena, Fig. 6 (right): the time-averaged breakdown location depending on the adverse pressure gradient set by the recompression at the wing trailingedge and/or by the blockage of the fin, the helical mode instability of the breakdown flow, quasi-periodic oscillations of the breakdown location, distortion of the incident vortex and vortex splitting, unsteady flow separation at the fin leading-edge, and possible coupling between the separated fin flow and/or fin elastic deformations with oscillations of the breakdown location. Among these, the dominant phenomenon causing fin buffeting is the quasiperiodic loading on the fin due to the helical mode instability of the leading-edge vortex breakdown flow.

2.4. Dominant frequency scaling

Characteristic parameters are of main importance for design or scaling tasks. Especially, a frequency parameter associated with vortex breakdown induced buffet loads is of specific interest to determine any alignment with eigenmode frequencies of wing or tail surfaces.

The shift in the dominant reduced frequency with angle of attack to lower values is plotted in Fig. 7. The quasi periodic velocity and induced surface pressure fluctuations, respectively, result from the helical mode instability of the flow downstream of vortex breakdown. The burst vortex core expands with increasing angle of attack and, therefore, the wavelength of the instability mode becomes larger and the corresponding frequency decreases. A universal frequency parameter can be derived using appropriate scaling quantities. Referring to velocity, the component normal to the leading-edge (U_∞ sinα) has to be considered. The length scale Ic must account for the vortex core expansion given approximately by scaling with the local half span (\sim x cot ϕ_W) and the shear layer distance ($\sim \sin^2 \alpha$). Using these relations leads to a scaling with the sinus of angle of attack α and the co-tangent of the wing leading-edge sweep ϕ_W . This scaling groups the

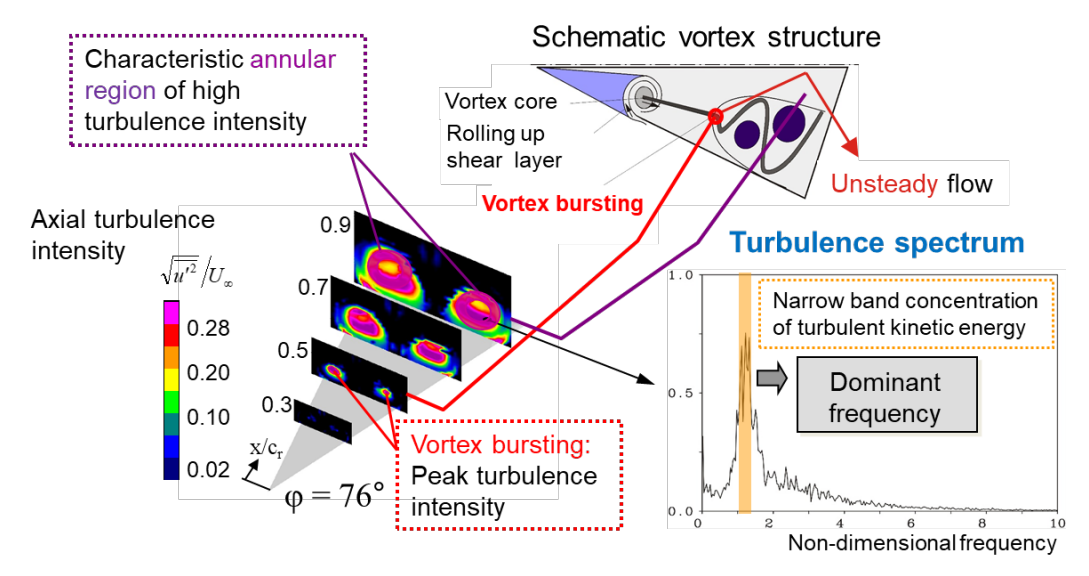


FIG 3. Characteristic delta wing turbulence intensity distributions and power spectral densities for the leading-edge vortex breakdown flow field; ϕ = 76°, Re_{Iµ} = 1.07 x 10⁶, α = 35.0°; I_µ: mean aerodynamic chord.

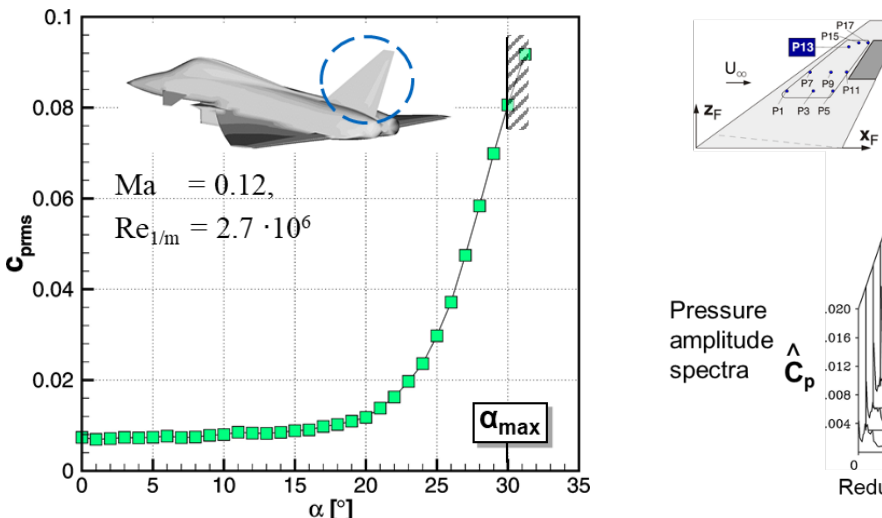


FIG 4. Surface averaged fin rms pressures as function of angle of attack; $U_{\infty} = 40 \text{ m/s}$, cf. [2].

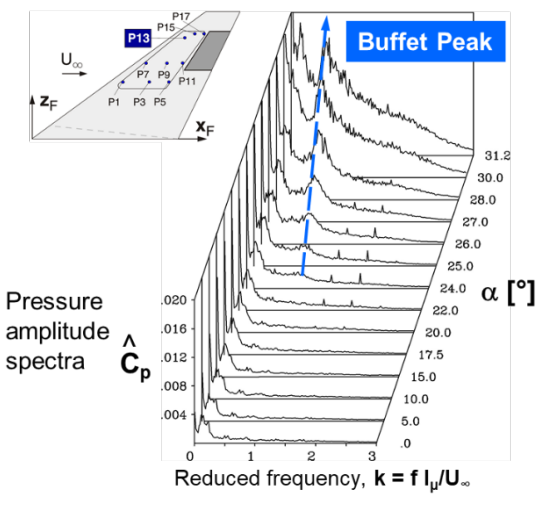


FIG 5. Pressure amplitude spectra taken at fin station P13 for various angles of attack; U_{∞} = 40 m/s, Ma = 0.12, Re_{1/m} = 2.7 x 10⁶, cf. [2].

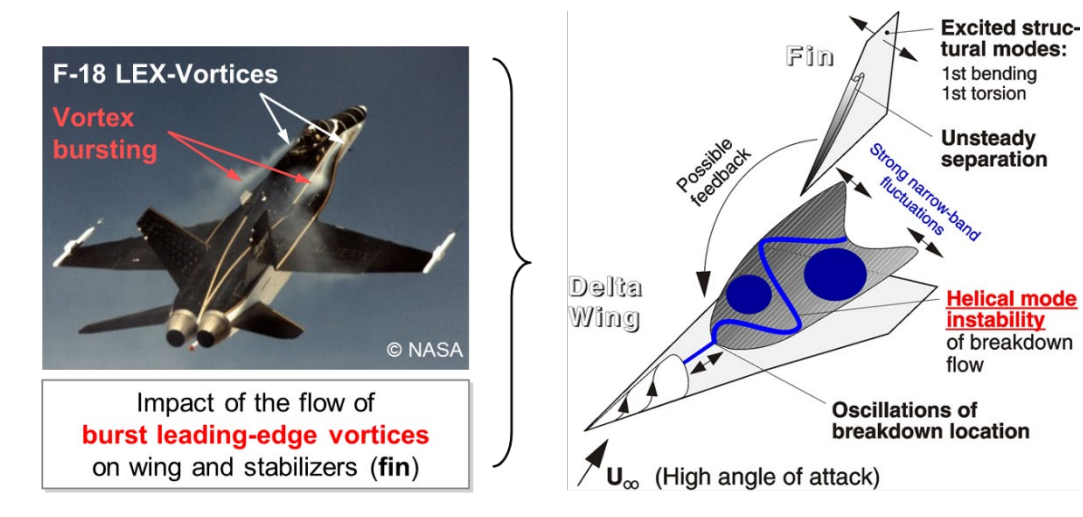


FIG 6. Phenomena related to fin buffeting: flight test visualization of F-18 LEX vortices bursting in front of the fins (left) and fluid–structure interactions of leading–edge vortex bursting and elastic fin (right); cf. [2].

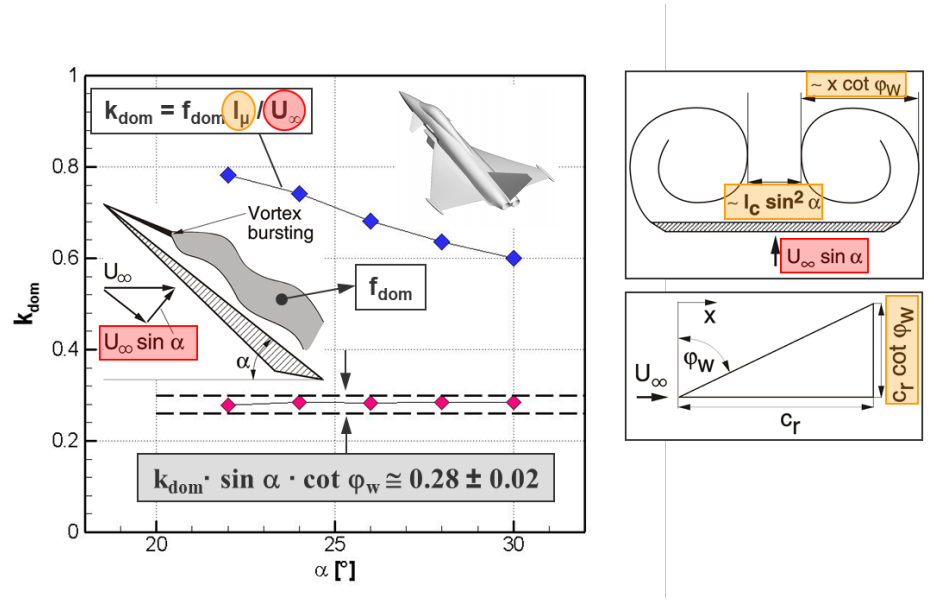


FIG 7. Dominant reduced buffet frequency k_{dom} (helical mode instability) as function of angle of attack based on amplitude pressure spectra of fin station P13 (cf. Fig. 5). Buffet load frequency parameter obtained by scaling k_{dom} with the sinus of angle of attack α and the cotangent of wing semi–span cot ϕ w; $U_{\infty} = 40$ m/s, $Re_{1/m} = 2.7 \times 10^6$; c_r : wing root chord, l_{μ} : mean aerodynamic chord, l_c : characteristic length; cf. [2].

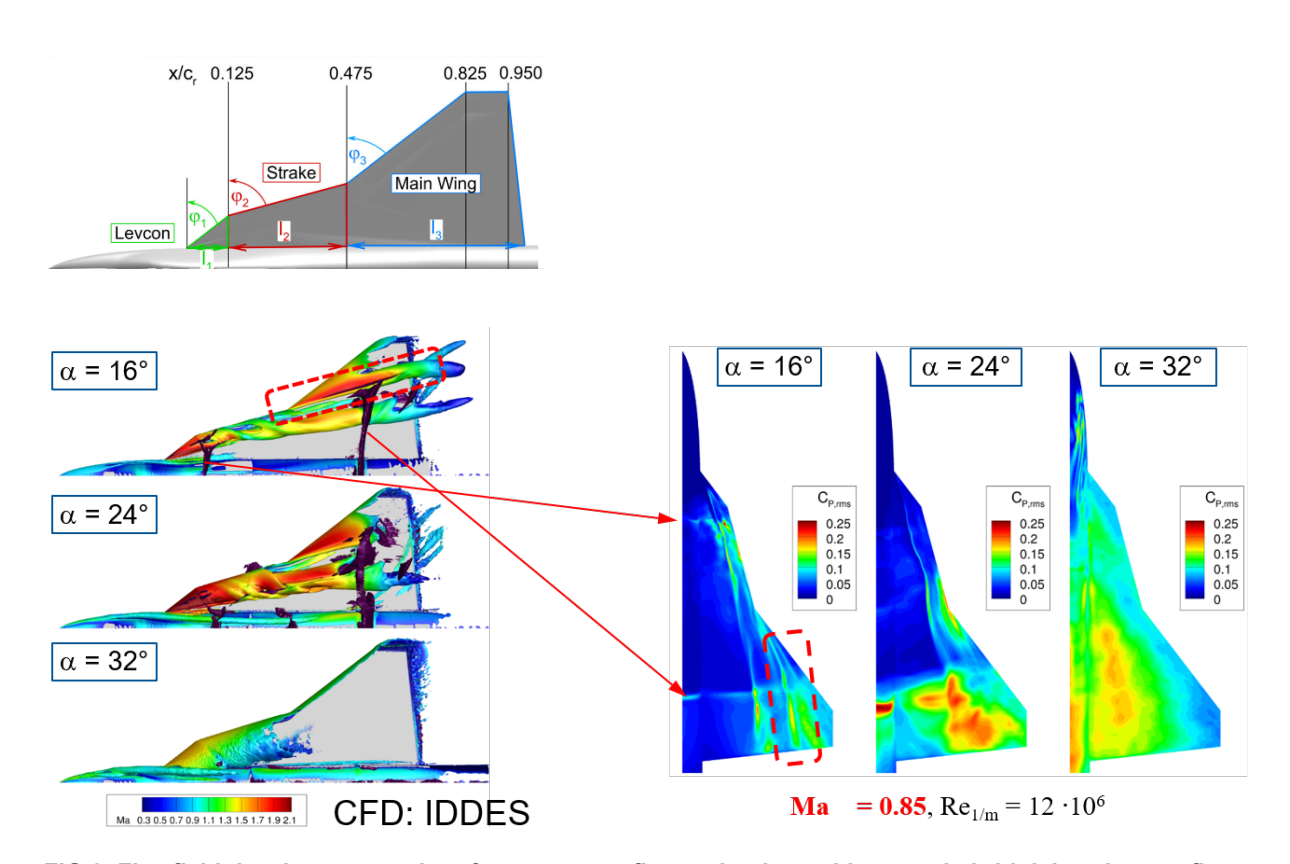


FIG 8. Flowfield development and surface pressure fluctuation intensities on a hybrid delta wing configuration at transonic conditions and high angles of attack obtained by Improved Delayed Detached Eddy Simulations (wing sections: leading-edge vortex controller element, Levcon, ϕ_1 = 52.5°; strake element, ϕ_2 = 75.0°; main wing, ϕ_3 = 52.5°).

values of the dominant reduced frequencies within a band of 0.28 ± 0.02 . Measurements on a variety of delta wing and strake-wing configurations substantiate the validity of the derived frequency parameter [2], [30]. For hybrid delta wings featuring multiple-swept leading-edge sections the relation can be also applied using an area weighted mean leading-edge sweep angle [31].

2.5. Wing vortex-shock interactions

At transonic operating conditions featuring wing regions of locally supersonic flow, compression shocks occur, which can interact with the vortices. Due to a vortex-shock interaction, the vortex experiences an abrupt pressure increase, which has a destabilizing effect and can lead to premature vortex bursting [5]. The underlying mechanisms show some similarities to those of shock-induced boundary layer separation. For vortex-shock interactions, a distinction is made between normal shock vortex interaction and oblique shock vortex interaction. Depending on the effect of the vortex-shock interaction, a distinction is also made between the so-called weak interaction, which does not lead to vortex bursting, and the strong interaction, which causes vortex bursting. The interaction with a normal shock is generally more critical and leads to forced vortex bursting, since the pressure rise across the shock is larger. The interaction between the vortex and the shock also leads to a deformation of the shock which exhibits as bulging of the shock wave in the upstream direction.

Fig. 8 presents numerical results based on Delayed Detached Eddy Simulations (DDES) for the flow field development on a hybrid delta wing configuration at high subsonic Mach number (Ma = 0.85, Re_{1/m} = $12 \cdot 10^6$) and moderate to high angles of attack ($\alpha = 16^{\circ}, 24^{\circ}, 32^{\circ}$). The wing planform consists of three elements, namely a leading-edge vortex controller (Levcon) section, a strake section and the main wing. Consequently, several leading-edge vortices (Levcon, strake and main wing vortices) are shed interacting with each other in downstream direction. Levcon and strake vortices merge to a propagating coherent vortex system influencing the main wing section. Details on those vortexvortex interactions are reported in Ref. [32]. In addition, upstream and downstream located shocks are present. For $\alpha = 16^{\circ}$, Mach number contours (Fig. 8 left) depict the evolution of the Levcon, strake and main wing leadingedge vortices. Local Mach numbers reach levels up to Ma ≈ 1.9 - 2.0. Upstream and downstream located strong normal shocks are clearly visible in spanwise direction. Both types of vortex-shock interactions occur: the weak and strong one. The first shock is located downstream of the canopy at the beginning of the strake section. The Levcon and strake vortices interact with this shock but remain stable. The second shock is located further downstream, at approximately 60% of the main wing root chord length. Both the strake and main wing vortices are affected by the second shock, exhibiting a strong interaction which contributes to subsequent vortex bursting. With raising angle of attack vortices increase in size and strength resulting in higher related velocities and associated Mach numbers. At $\alpha = 24^{\circ}$, a flow scenario can be detected exhibiting some main characteristics comparable to $\alpha = 16^{\circ}$, but shock induced vortex bursting for merged Levcon/strake and main wing vortices reveals much more pronounced. Post-stall effects are linked to $\alpha = 32^{\circ}$, where developed vortical flow structures are only present close to the apex while the entire main wing section is

determined by the Levcon/strake vortex breakdown flow inboard and irregular separated flow outboard.

For low-speed conditions (Fig. 3) it has been shown that the vortex breakdown flow with its high turbulence intensities gives rise to significant surface pressure fluctuations which may become severe for certain conditions. Fig. 8 (right) depicts the c_{p.rms} contours of the surface pressure fluctuations on the generic hybrid delta wing configuration. Local cp.rms maxima indicate the footprint of the impact of burst leading-edge vortices. At $\alpha = 16^{\circ}$ and α = 24°, inboard c_{p,rms} maxima refer to the breakdown flowfield of the merged Levcon/strake vortices while the outboard ones refer to the main wing vortex. Especially at α = 24°, c_{p,rms} maxima reach levels up to 25% spread over a larger wing area, thus, constituting a wing buffet relevant scenario. For α = 32°, the trace of high $c_{p,rms}$ values is concentrated inboard reflecting the impact of the merged and burst Levcon/strake vortex system, further revealing the spiral type vortex breakdown turbulent flow pattern.

3. SHOCK RELATED BUFFET

In the introduction it has been stated that transonic buffet is an unsteady shock-wave/boundary-layer interaction phenomenon, encountered e.g. for civil transport aircraft at edge of the flight envelope conditions. A risk of degraded handling qualities or structural failure may be caused by the interaction of the unsteady aerodynamic loads with the elastic wing structure. Certification regulations call for the absence of any buffet related structural vibrations within the flight envelope. The engineering challenges arising with the design of future wings pushing the limits of the flight envelope further require a thorough understandding of the mechanisms that govern the phenomenon.

As outlined in Sec. 2.5, the impact of shocks with the associated rise in static pressure may lead to dominant changes in the flow development. For certain flow conditions of high subsonic Mach numbers and angles of attack present at (supercritical) airfoils and wings, the shock induced pressure rise acting on the boundary layer may evoke flow separation downstream of the shock. The subsequent occurrence of a bubble type or open separation zone (extending to the trailing edge) has also an impact on the pressure field affecting in turn the shock. First, the shock is shifted further upstream due to the displacement of the growing area of separated flow, then the shock related pressure rise becomes alleviated and the flow is re-attaching with the shock position moving downstream until flow separation occurs again. Due to the separated flow unsteady characteristics a shock motion is developing. Therefore, on wings, quasi-periodic motions are related to chordwise and spanwise areas of attached and shock induced separated flow providing pronounced fluctuations of this area boundary. Consequently, the movement of the area boundary separating attached and separated flow along with the regions of separated flow themselves provide severe unsteady aerodynamic loads.

3.1. Unsteady flow field – Buffet impact

A typical buffet impact scenario for a transport aircraft wing is shown in Fig. 9 for the NASA CRM (Common Research Model) configuration (supercritical wing; aspect ratio: 9.0; taper ratio: 0.275; wing sweep: 35.0°). The corresponding wind tunnel model tested at cryogenic conditions for Mach and Reynolds number similarity represents a wing-body model equipped with a horizontal

tail plane. The design cruise condition is defined by a Mach number of Ma = 0.85, Reynolds number of Remac = 30 · 106 (based on freestream velocity and wing mean aerodynamic chord, mac) and a lift coefficient of $C_L = 0.5$. The buffet condition highlighted in Fig. 9 is due to an angle of attack of $\alpha = 5^{\circ}$. Applying the URANS setup described in Ref. [27], a buffet instability develops on the wing suction side. A series of six pressure coefficient snapshots linked to the buffet period T_{Buffet}, which is given here by 0.0067 s, are shown in Fig. 9a. A characteristic λ shaped two shock pattern develops on the wing upper side. Changes in the local surface pressures are shown for three distinct spanwise sections located at positions of $\eta = 0.60, 0.70, \text{ and } 0.80, \text{ Figs. 9b-d}$). The time instants (Fig. 9a) depict the chordwise and spanwise movement of the shock, thus, representing oscillations of the boundary separating attached and separated flow. Shock movement in chord direction is in the order of 5% to 8% of the local chord length linked to so called buffet cells which propagate in outboard direction. Fig. 9d reveals pronounced flow separation in the wing outboard area.

Further, a typical surface pressure distribution for a transonic transport aircraft wing (supercritical wing; aspect ratio: 9.302; taper ratio: 0.228; wing sweep: 30.0°) is also shown in Fig. 10 for the Airbus XRF-1 configuration [26]. It serves as the geometry of interest within the DFG (German Research Foundation) collaborative research unit FOR2895 [33]. Wing surface pressure data are obtained by Pressure Sensitive Paint (PSP) measurements conducted in the cryogenic European Transonic Windtunnel (ETW) facility to satisfy Mach number and Reynolds number similarity requirements [33]. Example results shown here are related to test conditions of Mach number Ma = 0.90. Revnolds number of Remac = 25 · 106 and angles of attack of α = 4°, 5°, and 6°, representing wing buffet conditions. As present for the CRM configuration, a λ-shaped shock pattern, typical for such wing geometries, is evident in the spanwise direction at all considered flow conditions (double shock in the inner region, converging in the center and shock front in the outer region). Typically, shocks are shifted upstream with increasing angle of attack, accompanied by an increase in shock intensity.

Pronounced shock oscillations in chordwise direction (5% to 10% of the local chord length depending on spanwise position) and propagation of buffet cells in spanwise direction can be observed (the region of which indicated by the outboard white dash line circles in Fig. 10).

3.2. Fluctuation intensities

Surface pressure fluctuation intensities are plotted in Fig. 11 (left) in terms of c_{p.rms} values revealing the area of largest pressure fluctuations acting on the XRF-1 upper side wing surface. The results shown here are based on URANS-SAS (SAS: Scale Adaptive Simulations) calculations for Ma = 0.84, Re_{mac} = 25 $\cdot 10^6$ and α = 5°. The respective numerical set-up is as follows: 80 Mio. cells; boundary layer: $y+,max \approx 0.32$, first layer height $1.5 \cdot 10^{-6}$ m with mac = 0.1965 m, 58 layers, cell growth rate 1.1 - 1.3; physical time step: 5 ·10⁻⁶ s). Results of the wing pressure distributions show reasonable agreement against the ETW measurement data comprising surface pressure data taken by pressure taps, Kulite sensors, PSP and unsteady PSP (iPSP). As expected local cp,rms maxima are attributed to the region of pronounced shock oscillations and outboard zones of separated flow. Levels of cp,rms are significantly high for the regions where the impact of spanwise propagating buffet cells becomes dominant. Thus, the wing area from half the span to the wing tip experiences locally concentrated large pressure fluctuation intensities. This flow scenario may evoke high accelerations at the wing tip due to structural response in wing bending modes.

3.3. Frequency characteristics and fluid modes

The sustained shock oscillation associated with waviness of the shock front and outboard convection of buffet cells may be linked to characteristic frequencies corresponding to appearance of dominant fluid modes. The related frequency content of the XRF-1 upper side wing surface pressure fluctuations is displayed using Power Spectral Density (PSD) distributions in the right part of Fig.11. Flow conditions are Ma = 0.84, and 0.90 at Re_{mac} = 25 \cdot 10⁶ and α = 4° and 5°. PSDs are plotted for the pressure fluctuations obtained at two Kulite stations the locations of which are depicted in the subfigure. The coloring of this subfigure refers to the mean pressure coefficient distribution at Ma = 0.90 and α = 5°. Spectral peaks denoted as buffet peaks ('3D buffet') can be detected in a broader frequency range linked to the spanwise buffet cell propagation. The related range of Strouhal numbers Sr or reduced frequencies k_{red} , respectively, is $k_{red} \approx 0.2 - 0.8$, using the freestream velocity and mean aerodynamic chord as reference quantities. The occurrence of buffet related frequencies in this range is also reported in various investigations, Refs. [15], [19], [20]. Mainly, a dependency on the wing sweep angle is documented [14]. Further, with increasing angle of attack buffet frequencies are shifted to lower values. Both wing sweep and angle of attack determines the wing leading-edge effective velocity and characteristic length scales. Consequently, a buffet related frequency parameter may depend on wing sweep, angle of attack, and ratio of taper to aspect ratios.

Besides this range of Strouhal numbers attributed to the spanwise oscillations of the wavy shock front an order of magnitude lower Strouhal number values can be linked to the chordwise shock oscillations seen in a sectional spanwise cut. Associated Strouhal numbers are in the range of 0.05 to 0.07. Dominant chordwise oscillations are linked to the points of inflection in the temporal spanwise variation of the wavy shock front.

Regarding fluid mode analysis based on the URANS-SAS results, Fig. 12 (left) presents exemplary mode patterns associated with the first four dominant modes obtained by applying Dynamic Mode Decomposition (DMD) for the XRF-1 wing upper side surface pressure fluctuations (Ma = 0.84, Re_{mac} = 25 ·10⁶, α = 5°). The mode pattern reveals the spanwise composition of fluctuation impacts of which the first dominant mode is at Sr \approx 0.32.

The schematic of the right part of Fig. 12 include main characteristic values for buffet related Strouhal numbers with respect to spanwise and chordwise shock dependent fluctuations, spanwise convection velocities, normalized with the freestream velocity U_{∞} , and buffet cell related wave lengths λ , normalized with the wing mean aerodynamic chord (mac).

As outlined for buffeting representing a dynamic aeroelastic problem the interaction of motion dependent and separation dependent unsteady aerodynamic forces is of major interest in analysis and classification of the problem. For airfoil (2D) buffet cases the influence of superimposed vibrations have been extensively studied both experimentally and numerically.



NASA CRM:

Wing aspect ratio: 9.0 Wing taper ratio: 0.275 Wing sweep, ϕ_{25} : 35.0°

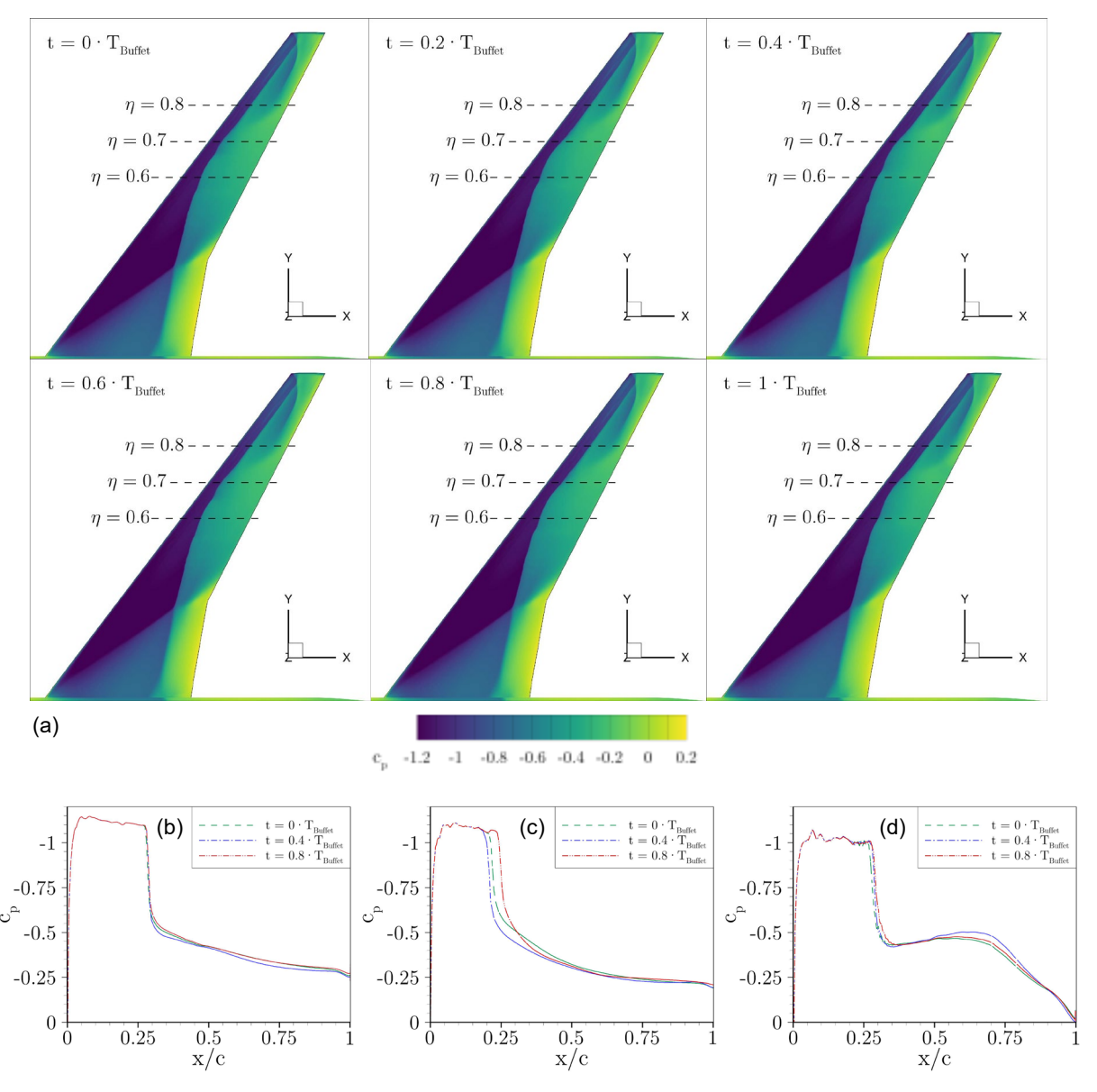


FIG 9. Time instants of wing surface pressure coefficient (c_p) distributions indicating the wing buffet cycle at the NASA CRM configuration; Ma = 0.85, Re_{mac} = 30 x 10⁶, α = 5.0°; T_{Buffet} refers to the buffet period; (a) Buffet cycle; (b), (c), (d) c_p distributions at 60%, 70% and 80% spanwise (η = y/s) stations; cf. [27].

©2025

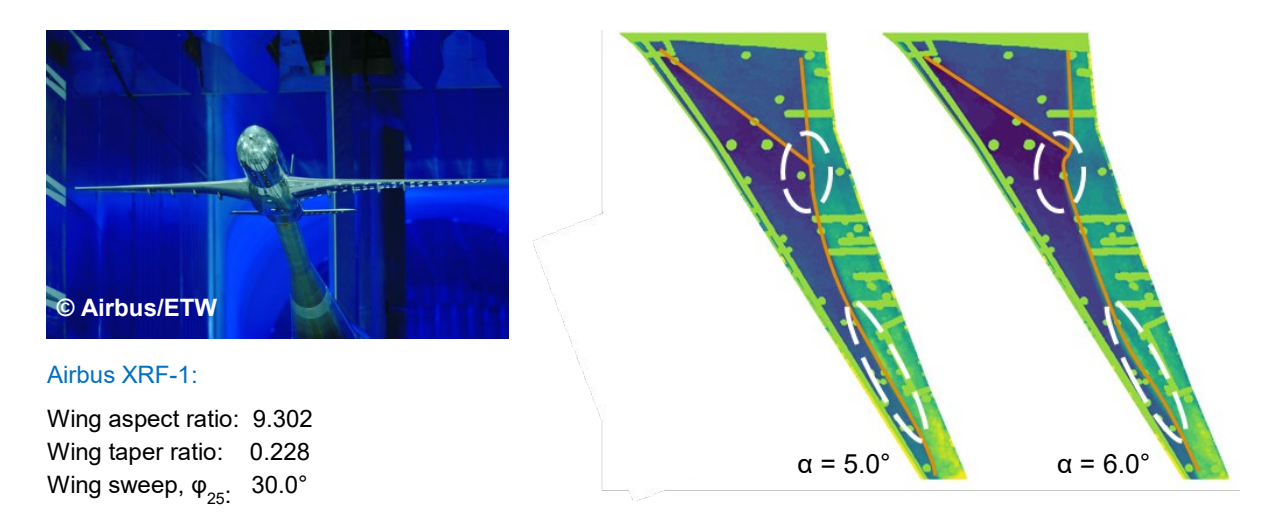


FIG 10. Mean surface pressure distributions on XRF-1 wing upper side based on PSP measurements indicating λ -shock topology; Ma = 0.90, Re_{mac} = 25 x 10⁶, α = 5.0° and 6.0°; cf. [26].

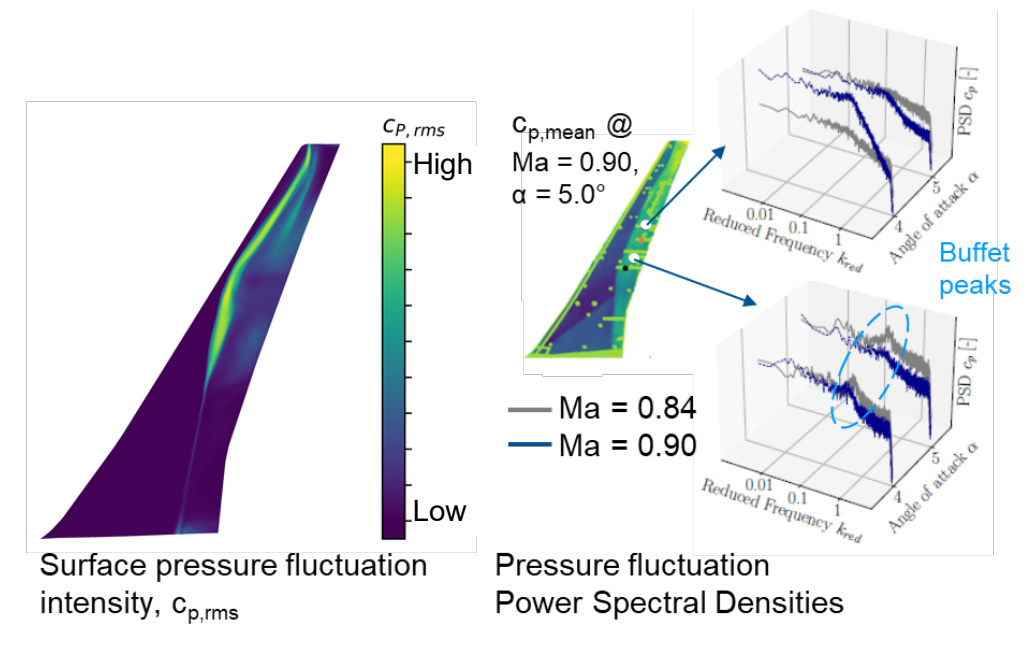


FIG 11. Unsteady surface pressure characteristics on XRF-1 wing upper side; left: $c_{p,rms}$ obtained by URANS-SAS calculations; Ma = 0.84, Re_{mac} = 25 x 10⁶, α = 5.0°; right: pressure fluctuation power spectral densities based on Kulite measurements.

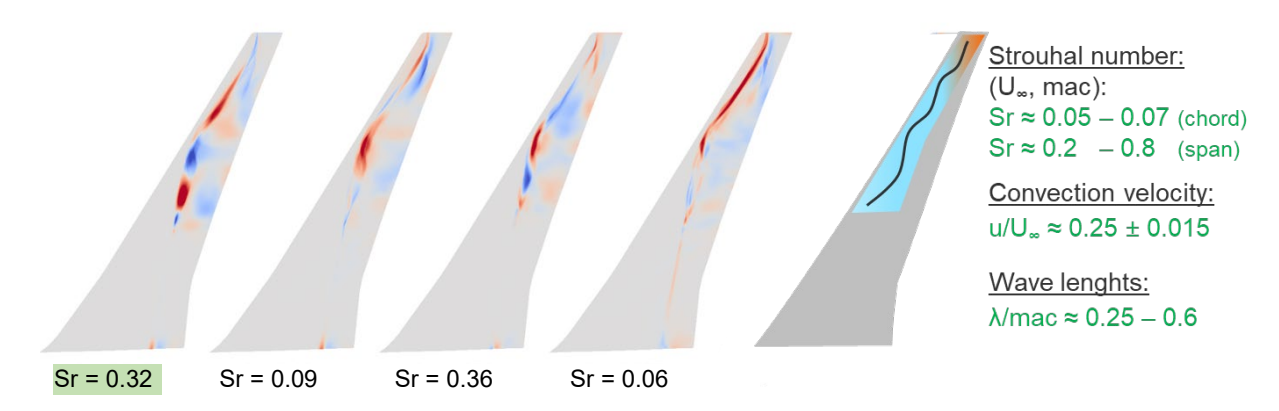


FIG 12. Mode and frequency features for unsteady surface pressures at XRF-1 wing upper side; left: DMD modes 1 – 4 based on URANS-SAS calculations; Ma = 0.84, Re_{mac} = 25×10^6 , α = 5.0° ; right: typical value ranges of characteristic frequencies and wave propagation.

When applying forced plunge or pitch motions, respectively, or if the airfoil is subjected to specifically tuned elastic suspensions with plunge and/or pitch degree of freedom, a full synchronization of the buffet frequency to the excitation for certain combinations of excitation frequency and amplitude is found, called 'lock-in effect' [21]. For wing geometries, those effects are less pronounced. Harmonic excitations of the wing or vibrations at structural eigen-frequencies may interact mainly with the high frequency characteristics attributed to the buffet phenomenon due to global fluid modes, while the low frequency behaviour is less affected. Mean surface pressure distributions are not influenced by vibrations with small amplitudes (e.g. not exceeding 0.05% of the wing span). Based on results of coupled fluid-structure simulations an initial (linear) structural response in the structural eigenmodes depends on the buffet frequency for all modes. This holds for structural modes with natural frequencies close to that of buffet in the nonlinear part of the response. A dependence on their respective structural frequencies and lower order bending modes is found for lower frequency structural modes in the nonlinear part of the response.

4. BUFFET ONSET CRITERIA

Due its relevance for design and certification a variety of buffet onset criteria or parameters, respectively, have been published over the years [34], [35]. Generally, the criteria are related to (i) integral mean aerodynamic data, (ii) local aerodynamic data and (iii) structural dynamics quantities (but in context of quasi rigid/stiff wind tunnel models). The first type of data concentrates on lift and pitching moment coefficients as function of angle of attack and the corresponding first and second order derivatives of the respective functions [36], [37]. Derived quantities like changes in the aerodynamic center are analyzed as well. The second group of data comprise trailing-edge pressures, intensities of surface pressure fluctuations and data on the region of separated flow [38]. The third data part include wing or tail tip accelerations and root wing bending moment fluctuations, respectively. These data are typically taken on quasi-stiff models (e.g. steel or aluminum structures, no structural dynamics scaling) as the vibration level on such models serves as a reasonable indicator of the buffet(ing) intensity. The application of some selected parameters is shown in this section, a comprehensive overview can be taken from the above mentioned references.

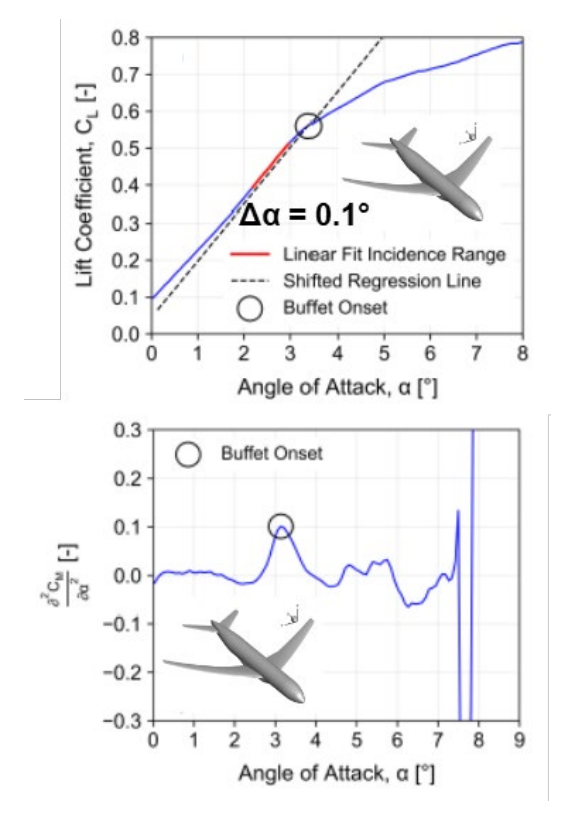
Referring to category (i), a widely used buffet onset criterion in industry is the so-called $\Delta \alpha = 0.1^{\circ}$ criterion [34]. As exemplarily indicated in Fig. 13a (upper subfigure) for the NASA CRM configuration, a straight line is drawn parallel to the linear part of the lift curve as function of angle of attack, shifted by $\Delta \alpha = 0.1^{\circ}$ to the right (dashed line). The criterion states that buffet onset can then be assumed at the intersection of this straight line with the lift curve. The idea behind is that shock induced flow separation, the region of which increases in size at higher angles of attack leading ultimately to buffet, is also indicated by a significant change in the C_L-curve slope. The circle in Fig. 13a points to the pronounced change in the lift curve slope. Similar considerations can be made for the pitching moment characteristics ('pitch break') but the pitching moment reference point must be taken into account for the analysis. Alternatively, a change in the aerodynamic center can be also used. Further, the lower subfigure of Fig. 13b shows the second order derivative curve of the pitching moment coefficient with angle of

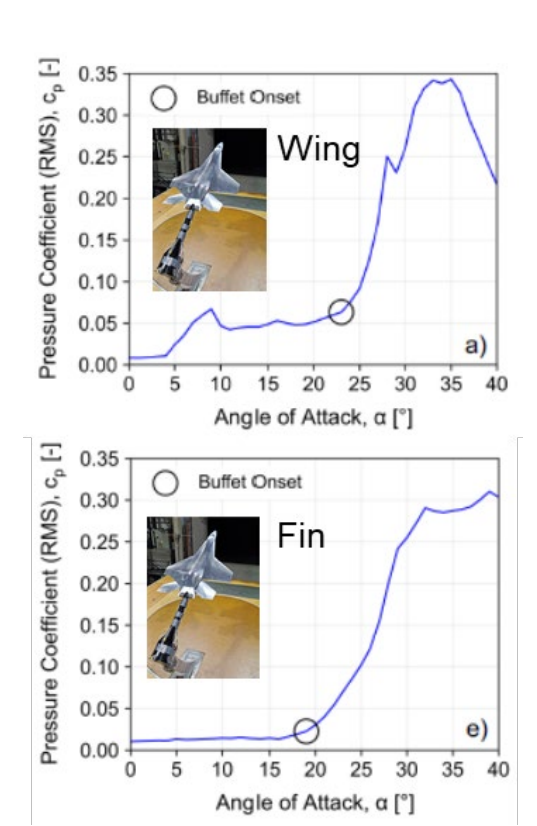
attack where the first pronounced maximum is attributed to buffet onset. For the chosen NASA CRM case this criterion is in good agreement to the $\Delta\alpha$ = 0.1° criterion substantiating here the consistency of criteria. A C_L x C_m criterion is established in Ref. [37] indicating that buffet(ing) onset can be linked to the maximum value of $(\partial^2 C_m/\partial^2 C_L)$.

A criterion within category (ii) focuses on the evolution of the trailing-edge pressure coefficient cp.TE. A correlation between the c_{p.TE} and buffet onset exhibits, that similar to the lift curve, cp,TE also changes approximately linearly with increasing angle of attack until at higher angles of attack a break in the curve occurs indicating flow separation. Again, a straight line parallel to the linear part of the curve is drawn and the intersection denotes a criterion for buffet onset. A value of $\Delta c_{p,TE} = -0.05$ is typically used as offset. For practical applications, the straight line is drawn parallel to the curve part with the smallest negative slope. There are a variety of further criteria [34]. For example, the area of the region of flow separation is taken suggesting that buffet onset can be assumed when the size of the flow separation area reaches 4% of the reference wing area. The value of 4% has been derived from a comparison with the $\Delta\alpha$ = 0.1° criterion at high subsonic freestream Mach numbers.

Surface pressure fluctuations in terms of c_{p,rms} values provides also a good indication of buffet onset as highlighted above for both high agility aircraft and transonic transport aircraft buffet. Fig 13b displays c_{p,rms} trends as function of angle of attack for surface pressure sensor positions on wing and fin of a strake-wing (leding-edge sweeps: 76°/40°) configuration at low-speed conditions [29], [30]. Both for wing and fin, a severe increase in pressure fluctuation intensity is detected that buffet onset is defined for exceeding a certain threshold (e.g. 3% or 5%) along with the gradient of the steep increase in c_{p,rms}.

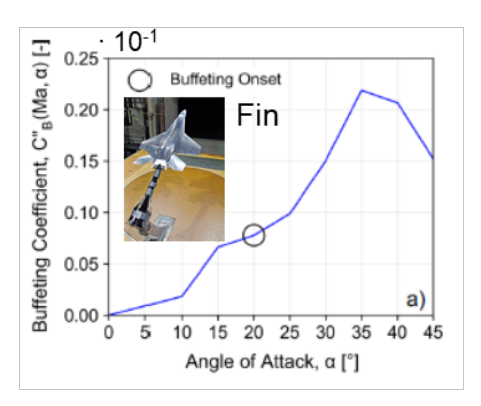
For category (iii), a buffet(ing) criterion is addressed introduced by D. Mabey [39]. This criterion is especially linked to wind tunnel testing of quasi-rigid/stiff models analyzing the structural response in the first bending mode of wing and/or tail surfaces given at those models. The buffet(ing) coefficient C"B is calculated with the known unsteadiness level due to wind tunnel turbulence as a reference to scale the model response determined e.g. from wing/fin root strain gauges. Below buffet onset the parameter C"B is found to be independent of angle of attack. The value C'B(Ma,0) is the portion of the model response caused by the tunnel turbulence intensity at zero angle of attack while C'B(Ma,a) is the one at varying angles of attack. The tunnel induced level in the response is subtracted to provide the buffeting coefficient C"B, see equation in Fig. 13c. A scaling factor can be added to C'B depending on the mass and stiffness of the model, and sensitivities of the root strain gauges and total damping. Assuming that a linear relationship exists between tunnel unsteadiness and wing response, C"B(Ma,a) refers to the response intensity linked to buffet(ing) onset. A certain threshold is defined to assign the level of intensity of C"B to the categories 'light', 'moderate' and 'heavy' buffeting. An example of the application of the C"_B(Ma,α) criterion is presented in Fig. 13c for the fin bending response of the strake-wing configuration [29]. The angle of attack associated with a level of moderate buffeting corresponds to the one for buffet onset of Fig. 13b (lower subfigure).





a) Gradient and curvature changes of trends in lift coefficient, c_L and pitching moment coefficient, c_M , as function of angle of attack; examples for NASA CRM, Ma = 0.85, Re_{mac} = 30 x 10^6 .

b) Surface pressure fluctuation intensities as function of angle of attack; examples for wing and fin sensor stations of TUM high agility configuration AWTM-F [29], Ma = 0.15, Re_{1/m} = 3.2×10^6 .



First wing bending response ('stiff model'): $C''_B(Ma,\alpha) = \sqrt{(C'_B(Ma,\alpha)^2 - C'_B(Ma,0)^2)}$

Buffeting criterion	Level of C"
Light	0.004
Moderate	0.008
Heavy	0.016

c) Buffeting intensity coefficient (criterion) based on measurements of wing root bending moment (fluctuations) obtained at quasi-stiff wind tunnel models as introduced in Ref. [39]; example for TUM high agility configuration AWTM-F [29], Ma = 0.15, Re_{1/m} = 3.2×10^6 .

FIG 13. Application examples of buffet(ing) on-set criteria.

5. CONCLUSIONS AND OUTLOOK

Buffeting denotes a dynamic aeroelastic problem with the interaction of unsteady aerodynamic forces, elastic forces and inertia forces. Classically, it is considered as a response problem in contrast to the stability problem 'flutter'. Buffeting constitutes a limit of the flight envelope and, therefore, has to be addressed in the aircraft design and certification process. The involved unsteady aerodynamic forces representing the structural excitation are referred to as buffet. They are composed by motion dependent aerodynamic forces due to the presence of structural eigenmode oscillations and flow separation dependent aerodynamic forces caused e.g. by leadingedge vortex bursting or presence of strong shocks oscillating themselves. Buffet and Buffeting have been studied for decades in wind tunnel tests, numerical simulations depending on the capability of fluid and structural modeling involved, and flight testing.

Severe Buffeting is associated with high dynamic loads depending on angle of attack and Mach number. Corresponding surface pressure fluctuation intensities expressed by root mean square (rms) values reach levels of up to 25% to 30%. Depending on the scenario of vortex breakdown induced buffet or shock induced buffet the unsteady loads exhibit narrow-band up to more broadband fluctuations associated with characteristics fluid instability mechanisms or fluid modes, respectively. Local peak loads of surface pressure fluctuations may experience large levels. The increase in power spectral density peaks of surface pressure fluctuations with angle of attack up to heavy buffet results in a factor of 5 to 12. Tip accelerations at high agility aircraft fins could raise to several hundred g's leading in the worst case to structural failure. The amount of data available for a large variety of generic and detailed geometries of wings and aircraft provide a thorough basis for design and evaluation.

Especially, the FOR2895 research unit concentrates on a detailed understanding on wing and horizontal tail buffet occurring on a representative long range transonic transport aircraft, the XRF-1 configuration. A unique data base is obtained in the European Transonic Windtunnel (ETW) for Mach and Reynolds number similarity employing latest optical measurement techniques. Recent tests include also forced vibrations aimed at analyzing the interaction of wing oscillations and buffet development, respectively, thus addressing the interaction of motion dependent and flow separation induced unsteady aerodynamic forces. This is accompanied by numerical simulations employing fluid structural coupling with oneand two-way approaches to shed light on dominating interaction mechanisms. Scaling relations for buffet frequencies at various geometric and flow conditions are also at focus. These findings will help to advance the understanding of the underlying physics of transonic buffet and ultimately inform future wing design.

Acknowledgements

The author gratefully acknowledge the Deutsche Forschungsgemeinschaft (DFG) for funding parts of this work within the framework of the research unit FOR 2895 (Unsteady flow and interaction phenomena at high speed stall conditions), subproject TP7, grant number BR1511/14-2, and the Helmholtz Gemeinschaft HGF, Deutsches Zentrum für Luft- und Raumfahrt DLR and Airbus for providing the XRF-1 wind tunnel model and financing the

XRF-1 wind tunnel measurements as well as public support to mature the test methods applied by DLR and FTW.

Contact address:

christian.breitsamter@tum.de

References

- [1] Collar, A. R.: The Expanding Domain of Aeroelasticity. J. Roy. Aeron. Soc., Bd. L pp. 613 636, 1946; s.a. Försching, H. W.: Grundlagen der Aeroelastik. Springer Verlag, Berlin, 1974.
- [2] Breitsamter, C.: Unsteady flow phenomena associated with leading-edge vortices. Progress in Aerospace Sciences, Vol. 44, No. 1, pp. 48 65, 2008. https://doi.org/10.1016/j.paerosci.2007.10.002.
- [3] Lee, B. H. K., Brown D., Zgela M., and Poirel D.: Wind tunnel investigations and flight tests of tail buffet on the CF-18 aircraft. Aircraft dynamic loads due to flow separation, AGARD-CP-483, Sorrento, Italy, April 1–6, pp. 1-1–26, 1990.
- [4] Luber W., Becker J., and Sensburg O.: The impact of dynamic loads on the design of military aircraft. Loads and requirements for military aircraft. AGARD-R-815, AGARD, Neuilly Sur Seine, France, pp. 8-1– 27, 1996.
- [5] Hirschel, E. H., Rizzi, A., Breitsamter, C., and Staudacher, W.: Separated and Vortical Flow in Aircraft Wing Aerodynamics. Springer Verlag, 2021. https://link.springer.com/book/10.1007/978-3-662-61328-3
- [6] Hummel, D.: Untersuchungen über das Aufplatzen der Wirbel an schlanken Deltaflügeln. Zeitschrift für Flugwissenschaften und Weltraumforschung, Band 13, pp. 158 – 168, 1965.
- [7] Gursul, I. and Xie, W.: Buffeting Flows over Delta Wings, AIAA Journal, Vol. 37, No. 1, pp. 58 – 65, 1999. https://doi.org/10.2514/2.664
- [8] Meyn L. A. and James K. D.: Full-scale wind tunnel studies of F/A-18 tail buffet. Journal of Aircraft, Vol. 33, No. 3, pp. 589 – 595, 1996. https://doi.org/10.2514/3.46986
- [9] Hauch, R. M., Jacobs, J. H., Dima, C., and Ravindra, K.: Reduction of vertical tail buffet response using active control. Journal of Aircraft, Vol. 33, No. 3, pp. 611 – 622, 1996. http://doi.org/10.2514/3.46990
- [10] Breitsamter, C.: Aerodynamic Active Control for Fin-Buffet Load Alleviation. Journal of Aircraft, Vol. 42, No. 5, pp. 1252 – 1263, 2005. https://doi.org/10.2514/1.8174
- [11] Breitsamter, C. and Schmid, A.: Airbrake-Induced Fin-Buffet Loads on Fighter Aircraft. Journal of Aircraft, Vol. 45, No. 5, pp. 1619 – 1630, 2008. https://doi.org/10.2514/1.33969
- [12] Katzenmeier, L., Vidy, C., and Breitsamter, C.: Using a Proper Orthogonal Decomposition Representation of the Aerodynamic Forces for Stochastic Buffeting Prediction. J. of Fluids and Structures, Vol. 99, 2021. https://doi.org/10.1016/j.jfluidstructs.2020.103178
- [13] Iovnovich, M. and Raveh, D. E.: Numerical Study of Shock Buffet on Three-Dimensional Wings. AIAA Journal, Vol. 53, No. 2, pp. 449 – 463, 2015. https://doi.org/10.2514/1.J053201

- [14] Paladini, E., Dandois, J., Sipp D., and Robinet, J.-Ch.: Analysis and Comparison of Transonic Buffet Phenomenon over Several Three-Dimensional Wings. AIAA Journal, Vol. 57, No. 1, pp. 379 – 396, 2019. https://doi.org/10.2514/1.J056473
- [15] Masini, L., Timme, S., and Peace, A.: Analysis of a Civil Aircraft Wing Transonic Shock Buffet Experiment. Journal of Fluid Mechanics, Vol. 884, A1, pp. 1 – 42, 2020. https://doi.org/10.1017/jfm.2019.906
- [16] Crouch, J., Garbaruk, A., and Strelets, M.: Global instability in the onset of transonic-wing buffet corrigendum. Journal of Fluid Mechanics, 901, E1, 2020; https://doi.org/10.1017/jfm.2020.557
- [17] He, W. and Timme, S.: Triglobal infinite-wing shock-buffet study. J. Fluid Mechanics, Vol. 925, A27, 2021. https://doi.org/10.2514/1.J053201
- [18] Timme, S.: Global Instability of Wing Shock-Buffet Onset. Journal of Fluid Mechanics, Vol. 885, 2020. https://doi.org/10.1017/ifm.2019.1001
- [19] Ohmichi, Y. and Hashimoto, A.: Numerical Investigation of Transonic Buffet on a Three-Dimensional Wing Using Incremental Mode Decomposition. AIAA Paper 2017-1436, 2017. https://doi.org/10.2514/6.2017-1436
- [20] Ehrle, M., Waldmann, A., Lutz, T., and Krämer, E.: Simulation of transonic buffet with an automated zonal DES Approach. CEAS Aeronautical Journal, Vol. 11, pp. 1025 – 1036, 2020. https://doi.org/10.1007/s13272-020-00466-7.
- [21] Raveh, D. E. and Dowell, E. H.: Frequency Lock-In Phenomenon for Oscillating Airfoils in Buffeting Flows. Journals of Fluids and Structures, Vol. 27, No. 1, pp. 89 – 104, 2011. https://doi.org/10.1016/j.jfluidstructs.2010.10.001
- [22] Raveh, D. E. and Dowell, E. H.: Aeroelastic Responses of Elastically Suspended Airfoil Systems in Transonic Buffeting Flows. AIAA Journal, Vol. 52, No. 5, pp. 926 934, 2014. https://doi.org/10.2514/1.J052185
- [23] Scharnowski, S., Kokmanian, K., Schäfer, C., Baur, T., Accorinti, A., and Kähler, C. J.: Shock-buffet analysis on a supercritical airfoil with a pitching degree of freedom. Experiments in Fluids, Vol. 63:93, 2022. https://doi.org/10.1007/s00348-022-03427-4
- [24] Zahn, R., Winter, M., Zieher, M., and Breitsamter, C.: Application of a long short-term memory neural network for modeling transonic buffet aerodynamics. Aerospace Science and Technology, Vol. 113, 2021. https://doi.org/10.1016/j.ast.2021.106652
- [25] Zahn, R., Weiner, A. and Breitsamter, C.: Prediction of Wing Buffet Pressure Loads Using a Convolutional and Recurrent Neural Network Framework. CEAS Aeronautical Journal, Vol. 15, pp. 61 – 77, 2024. https://doi.org/10.1007/s13272-023-00641-6
- [26] Zahn, R.: Deep Learning Approaches for Transonic Aerodynamic Buffet Analysis. Dissertation, Technical University of Munich, 2024. https://mediatum.ub.tum.de/1719360
- [27] Zahn, R., Zieher, M., and Breitsamter, C.: Deep Learning Framework for Predicting Transonic Wing Buffet Loads Due to Structural Eigenmode-Based Deformations. Aerospace 2025, Vol. 12, No. 5, 415. https://doi.org/10.3390/aerospace12050415

- [28] Stegmüller, J., Katzenmeier, L., and Breitsamter, C.: Horizontal tail buffeting characteristics at wing vortex flow impact. CEAS Aeronautical Journal, Vol. 13, pp. 779 – 796, 2022. https://doi.org/10.1007/s13272-022-00593-3
- [29] Stegmüller, J., Molz, A., Garcia-Guillen, P., and Breitsamter, C.: Flow field analysis of a high agility type aircraft aeroelastic wind tunnel model. Aerospace Science and Technology, Vol. 162, 2025. https://doi.org/10.1016/j.ast.2025.110177
- [30] Hartl, P., Stegmüller, J., Hayböck, S., Molz, A., and Breitsamter, C.: Experimental Investigations of a Wind Tunnel Model for the Analysis of Fluid-Structure Interaction Caused by the Influence of Leading-Edge Vortex Systems. DLRK2023, Paper 610509, 2023. https://www.dglr.de/publikationen/2023/610509.pdf
- [31] Sedlacek, D., Heckmeier, F. M., Usbek, A., and Breitsamter C.: Analysis of Vortex Burst Phenomena on Generic Hybrid Delta Wing Planforms at Subsonic Speeds. NNFM, Vol. 151, pp. 282 – 291, 2021. https://doi.org/10.1007/978-3-030-79561-0 27
- [32] Pfnür, S. and Breitsamter, C.: Leading-Edge Vortex Interactions at a Generic Multiple Swept-Wing Aircraft Configuration. Journal of Aircraft, Vol. 56, No. 6, 2019. https://doi.org/10.2514/1.C035491
- [33] Waldmann, A., Ehrle, M. C., Kleinert, J., Yorita, D., and Lutz, T.: Mach and Reynolds number effects on transonic buffet on the XRF-1 transport aircraft wing at flight Reynolds number. Experiments in Fluids Vol. 64:102, 2023. https://doi.org/10.1007/s00348-023-03642-7
- [34] Breitenstein, C.: Overview of criteria to estimate aerodynamic limits of the flight envelope of a transonic aircraft based on RANS simulations. CEAS Aeronaut Journal, Vol. 14, pp. 913 926, 2023. https://doi.org/10.1007/s13272-023-00685-8
- [35] Bérard, A. and Isikveren, A.T.: Conceptual design prediction of the buffet envelope of transport aircraft. Journal of Aircraft, Vol. 46, No. 5, pp. 1593–1606, 2009. https://doi.org/10.2514/1.41367
- [36] Lawson, S., Greenwell, D., and Quinn, M. K.: Characterisation of Buffet on a Civil Aircraft Wing AIAA Paper 2016-1309, 2016. https://doi.org/10.2514/6.2016-1309
- [37] Sousa, R. S., Girardi, R. D., and Annes da Silva, G. D.: A new criterion for transonic buffeting onset estimation. AIAA Paper 2017-4231, 2017. https://doi.org/10.2514/6.2017-4231
- [38] Benoit, B. and Legrain, I.: Buffeting prediction for transport aircraft applications based on unsteady pressure measurements. AIAA Paper 87-2356, 1987. https://doi.org/10.2514/6.1987-2356
- [39] Mabey, D. G.: Buffeting Criteria for a Systematic Series of Wings. Journal of Aircraft, Vol. 26, No.6, pp. 576 581, 1989. https://doi.org/10.2514/3.45805